Investigation of wave-driven hydroelastic interactions using numerical and physical modelling approaches

Brown, S. A.; Xie, N.; Hann, M. R.; Greaves, D. M.

Published in:
Applied Ocean Research

DOI:
10.1016/j.apor.2022.103363

Publication date:
2022

Investigation of wave-driven hydroelastic interactions using numerical and physical modelling approaches

S.A. Brown[a,*], N. Xie[a,1], M.R. Hann[a], D.M. Greaves[a]

[a]*School of Engineering, Computing and Mathematics, University of Plymouth, Plymouth, United Kingdom*

Abstract

Wave-driven hydroelasticity is of great importance to a wide range of applications within offshore and coastal engineering. Harnessing the benefits of hydroelasticity or minimising its impacts, depending on the application, has recently led to substantial investment in research effort in this field. However, the complex and strongly-coupled nature of the problem generally make the impacts very case specific, highlighting the importance of accurate numerical tools for assessing the impact on a case-by-case basis. Therefore, this study aims to provide novel experimental data to assist with the development of a coupled numerical methodology for simulating fully nonlinear hydroelastic interactions with highly-flexible floating structures. Novel physical data from a laboratory campaign conducted at the University of Plymouth is presented, and used as a reference for assessing the capabilities of an existing coupled numerical approach. The numerical model is a partitioned approach based within the open-source computational fluid dynamics software OpenFOAM and consisting of a two-phase fluid solver; a linear solid model for small deformations solved via the block-coupled method; and strongly-coupled through the Dirichlet-Neumann method with dynamic Aitken under-relaxation. The numerical model is shown to capture well the wave-induced deformation, and the qualitative differences between structures of varying dimensions. However, the high computational cost limits the scope of this work to 2-D, and future work should focus on optimising the approach to allow for application in 3-D problems.

Keywords:
Hydroelasticity, Fluid-Structure Interaction, Physical Modelling, OpenFOAM, Dam Break

1. Introduction

Hydroelasticity, the interaction of a fluid flow with an elastic structure, is a process which is expanding in significance in the field of coastal and offshore engineering due to its importance in a wide range of practical problems. Examples of potential applications in the marine environment include but are not limited to: free-fall lifeboats in launch and recovery operations [50]; Very Large Floating Structures (VLFSs) such as floating breakwaters [13], floating runways [15] and artificial floating islands [65]; ice sheet dynamics [23]; large marine mammal interactions with turbine blades [16]; and piezoelectric structures [45]. Substantial research effort is currently being invested into Offshore Renewable Energy (ORE), in particular, aimed at exploiting the potential benefits of hydroelasticity as the industry experiences significant development and priority backing from governments worldwide due to the ongoing climate crisis [25]. Flexible membranes have been proposed as a possible solution to achieve a step change in cost for Wave Energy Converters (WECs) due to the relatively low price of the materials [29], and the potential size reduction of devices [32]. In alternative ORE fields, the utilisation of elasticity in key components, such as turbine blades for tidal and Floating Offshore Wind (FOW) devices, has the potential to mitigate fatigue loading [58] but simultaneously risks becoming unsteady under specific inertial conditions [59]. Hence, understanding the mechanisms behind hydroelasticity is key to improving the lifespan of devices, which, in return, will drive down the Levelised Cost of Energy (LCOE) and, consequently, create a more viable option for a sustainable future.

Physical modelling has a key role to play in addressing this knowledge gap, and determining the impacts of hydroelasticity, since it can provide data on the deformation of a structure under specific hydrodynamic conditions. There are, however, a number of fundamental issues associated with physical modelling that make it a significant challenge for highly-flexible floating homogeneous structures, which are the subject of the present study. For example, non-invasive measurement techniques for the deformations must be utilised since any effect on the hydrodynamics will likely affect the response, and integrating sensors within structures of a single material without altering the material properties is a non-trivial problem. Accurate quantification and description of highly non-linear

*Corresponding author
Email address: scott.brown@plymouth.ac.uk (S.A. Brown)
[1]Present Address: Department of Engineering, Saipem (UK) Ltd., Kingston-upon-Thames, United Kingdom

free-surface processes that floating structures are routinely exposed towards, such as green water, wave breaking and ventilation, is another significant challenge, and the sensitivity of these processes to initial conditions significantly reduces the repeatability of the problem. The station-keeping method is another crucial consideration since it must be rigid, whilst causing minimal influence on the hydrodynamics and structural deformation.

Numerical modelling has the potential to compliment physical modelling campaigns through highly detailed analysis on the internal dynamics of the structure, whilst offering a solution to some of the aforementioned limitations of laboratory techniques. For instance, fixings and measurements can be defined without the need for infrastructure or instrumentation, and incident flow conditions can be more closely controlled, removing any repeatability concerns. Hydroelasticity, however, presents a complex challenge due to the strongly coupled nature of the problem, and hence accurate, validated and robust numerical software is still under active development. A considerable number of approaches of varying degrees of fidelity have been suggested for wave-driven, floating hydroelastic applications. Lower-fidelity models, based on potential flow theory are a commonly used option. These approaches typically couple the surface-discretised Boundary Element Method (BEM) for the fluid domain, with structural response formulations such as the Kirchhoff-Love elastic plate [37, 19] or Euler-Bernoulli Beam Theory [51], solved via the Finite Element Method (FEM), a more generalised but memory intensive, volume-discretisation. The low computational cost of these potential flow approaches make them an attractive option for hydroelasticity in particular, due to iterative procedures required for the strong coupling between the mesh and the solid. They have limitations in their application, however, since it is not possible to model highly nonlinear processes, especially when flow separation occurs.

High-fidelity Navier-Stokes are alternative approaches that offer a more generalised solution for the fluid dynamics, capable of capturing strongly non-linear processes that may occur in a hydroelastic interaction, such as aeration [1]; wave breaking [21]; overtopping [23];and slamming [46]. This generalisation, however, comes at significant additional computational cost. High-fidelity approaches can be sub-categorised into mesh-based and particle-based approaches, both of which solve the Navier-Stokes equations but using a Eulerian and Lagrangian formulation, respectively. Mesh-based approaches are generally considered the more established method and have been thoroughly demonstrated in a large range of marine applications [14, 62, 33]. Use of particle-based methods such as Smoothed Particle Hydrodynamics (SPH) [17] and the Moving Particle Semi-Implicit (MPS) method [31], however, have recently increased in popularity for wave-structure interaction problems since they benefit from simplified free-surface treatment especially in violent separated flows, and avoid mesh-related complications around complex geometries [36]. These potential advantages, however, come at further computational cost [36] due to low convergence rate; constraints on the maximum timestep; and the requirement to recalculate the near neighbour particles at every timestep. In hydroelastic applications, Navier-Stokes approaches are most often coupled with mesh-based solutions for the structural mechanics, solved via the FEM [66]. In applications where the structure may separate, however, such as breakup of ice sheets, the use of the particle-based Discrete Element Method (DEM) for the structural mechanics can be beneficial since it avoids potential discontinuities in the mesh [33, 20]. Furthermore, coupling between particle-based fluid solvers and Lagrangian approaches for the structural deformation, such as the DEM [64] and total Lagrangian formulation [43], have been demonstrated recently. These particle-particle coupled approaches are in their infancy, however, compared with the more classical mesh-based approaches, and consequently the method's capabilities are less well known. Hence, fully Lagrangian approaches will require rigorous validation for accuracy, convergence, stability and conservation properties [18] before they become an established option for hydroelastic simulations.

Primarily motivated by wave energy and inflatable vessel applications, the aim of this study is to provide novel experimental data to assist with the development of a high-fidelity, coupled numerical methodology for simulating fully nonlinear hydroelastic interactions with highly-flexible floating membrane structures. New physical data from a targeted laboratory campaign conducted at the University of Plymouth are presented in this study, alongside comparison with numerical simulations. Physical modelling techniques for floating hydroelastic interactions typically draw on experience from ship modelling procedures, and hence a common approach is to sub-divide the object into a number of segments that are connected by a beam [38, 60]. The intricacy of this approach, however, complicates numerical model validation due to the additional uncertainty associated with the interaction of the adjoining segments. Hence, validation is better suited to test cases which can be more easily analysed, such as flexible floating structures constructed of a single homogeneous material in well-defined wave environments. The number of previous laboratory studies with such conditions are limited, however, but examples include wave basin experiments of long flexible structures [63], and wave-ice interaction using ice tanks [19] or modelled through elastic discs [42] and viscoelastic covers [54]. These studies typically utilised materials that are considerably stiffer than used in wave energy applications. This study therefore presents a physical modelling campaign designed to provide valuable data for hydroelastic interactions of highly-flexible floating structures, whilst supporting validation procedures by ensuring that the laboratory configuration can be consistently reproduced with the numerical approach. A particular challenge for physical modelling of homogeneous materials is the measurement of structural displacement since integra-

tion of sensors into the model is non-trivial. Hence, in the present work measurements are taken via non-contact optical motion tracking. The presented test cases exhibit linear motions, time-harmonic conditions, a single material of homogeneous material with low modulus of elasticity and restraints on the structure's motion. Although the long-term aim is to be able to utilise numerical codes in fully non-linear hydrodynamic conditions (hence the use of a high-fidelity fluid solver), in this work structures of varied dimensions are assessed in near-linear monochromatic wave conditions for simplicity to allow for thorough comparison with the numerical model.

Mesh-based approaches are utilised for both the fluid and structural components of the numerical aspect of this study, and high-fidelity modelling to allow for generalised use in marine applications in the future. In isolated mesh-based Computational Solid Mechanics (CSM) applications, traditionally the well established FEM is applied [3, 24] taking advantage of a complete mathematical framework and well established convergence properties. On the other hand, mesh-based Computational Fluid Dynamics (CFD) codes are often based on the Finite Volume Method (FVM), which is more complex to complete but provides improved conservation properties. The discretisation method discrepancy makes it convenient to use a partitioned approach for a Fluid-Structure-Interaction (FSI) problem, where the flow and structure are solved independently on two separate meshes with coupling achieved through communication on the shared boundaries. This method benefits from allowing for specialist fluid and solid codes to be exploited for the hydrodynamics and structural mechanics, respectively, but is solved sequentially at each timestep. Hence, in principle, the partitioned approach is more computationally efficient than a monolithic approach (where the flow and structure are solved simultaneously within a single solver), but this comes at the expense of accuracy and stability [41]. FVM-FEM coupled, partitioned approaches have previously been successfully demonstrated for two-phase flows [30, 12], but recently the use of FVM for both the fluid and structural mechanics has been actively investigated [11]. This approach allows for integration within a single base code, and as problems increase in size and complexity, has potential benefits in computational load balancing as well as a more intuitive code structure and interface for users [10].

OpenFOAM, which is the basis of the numerical model used in this study, is an example of a software based on the FVM and primarily applied for CFD problems, which has recently seen substantial expansion in the area of solid mechanics and FSI. Building upon previous demonstrations for large deformations [57], a partitioned FSI solver for single phase, incompressible flows was introduced into the FOAM-Extend fork of the code. This has since been superseded by a series of FSI toolboxes [56] released through the Extend-bazaar platform [44] that provide the user with considerable further options and functionality for fluid, solid and coupling algorithms. These toolboxes have been further extended for two-phase flows [22, 40] and recently has been made publicly available as part of the latest iteration of the FOAM-Extend FSI toolboxes named `solids4foam` [10].

In this study, numerical results obtained from the `solids4foam` toolbox are presented alongside the novel physical data, with modifications to allow for relaxation zones to improve the quality of wave generation and absorption. The use of a FVM-FVM coupled code deviates from the more commonly applied FVM-FEM coupled approach, but previously it has been successfully demonstrated for wave-ice sheet interactions [23], which exhibits similarities with the present application. Sea ice, however, tends to be considerably stiffer and inhomogeneous [54] compared with the highly flexible floating structures considered here, and hence the responses are anticipated to be considerably larger in the present work. Furthermore, the focus here will be on the structure's response to wave-forcing, rather than the wave reflection and overwash as presented by Huang et al. [23].

This article is organised such that Section 2 provides details on the numerical approach, with mathematical descriptions of the functionality utilised in this study. In Section 3 an established benchmark for the interaction of a two-phase dam-break is considered for validation, with comparison against existing physical and numerical data. Section 4 focuses on wave-induced hydroelasticity on floating structures, presenting both the laboratory campaign and the numerical modelling comparison. Finally in Section 5 the conclusions are drawn.

2. Numerical Method

The numerical model used for this study is the `solids4foam` toolbox [10] which is based in the FOAM-Extend 4.1 fork of the open-source, high fidelity CFD software OpenFOAM. Developed by Cardiff et al. [10], the toolbox is a modular framework for simulating solid mechanics and FSI problems, which is designed to be intuitive to use, maintain and extend. The FSI simulations considered in this work can be considered as three components, each of which will be discussed separately: the fluid solver; the structural solver; and the coupling procedure between the fluid and structural domains.

2.1. Fluid Solver

The hydrodynamics are solved on a deforming mesh, which adapts according to the instantaneous position of the structure. In this study, the hydrodynamics are solved using a version of the `interFoam` solver [52], which has been modified for wave generation and absorption via the relaxation zone technique utilising the `waves2Foam` toolbox [28]. Previously, this approach has been thoroughly validated for fixed [6, 49] and rigid floating structures

[7, 48], and recently demonstrated in sea-ice hydroelastic applications [23]. The model solves the two-phase, incompressible, Reynolds-Averaged Navier-Stokes (RANS) equations

$$\frac{\partial(\rho\mathbf{u})}{\partial t} + \nabla\cdot(\rho\mathbf{u}\mathbf{u}) = -\nabla p + \nabla^2(\rho\nu\mathbf{u}) + \rho\mathbf{g}, \quad (1)$$

$$\nabla\cdot\mathbf{u} = 0, \quad (2)$$

where p is the pressure, $\mathbf{u} = (u, v, w)$ is the fluid velocity and $\mathbf{g}$ is acceleration due to gravity [52]. The fluid density, ρ, and kinematic viscosity, ν are determined using the Volume Of Fluid (VOF) interface capturing scheme

$$\frac{\partial\alpha}{\partial t} + \nabla\cdot(\mathbf{u}\alpha) = 0, \quad (3)$$

$$\rho = \rho_0\alpha + \rho_1(1-\alpha), \quad (4)$$

$$\nu = \nu_0\alpha + \nu_1(1-\alpha), \quad (5)$$

where α is an indicator function representing the phase fraction of each mesh cell, and subscripts 0 and 1 represent air and water, respectively [52]. As explained by Rusche [52], the solver uses an artificial compression term (C_α) when solving the transport equation for the volume fraction (equation 3), and this is set to $C_\alpha = 1$ in the present study. The Navier-Stokes equations (equations 1 and 2) are solved using a first-order temporal scheme (Backwards Euler) and second-order spatial schemes (Central Differencing and MUSCL) with the pressure-velocity coupling achieved via the Pressure Implicit with Splitting of Operators (PISO) algorithm [27] using 3 correctors. In this work, the flow is considered to be laminar throughout.

2.2. Structural Model

A linear elastic model is utilised for the structural model based on Hooke's law [11]. Assuming an arbitrary body of volume Ω which is bounded by surface Γ with outward facing normal, $\mathbf{n}$, the conservation of linear momentum can be expressed as

$$\int_\Omega = \nabla\cdot\boldsymbol{\sigma}d\Omega = \oint_\Gamma \mathbf{n}\cdot\boldsymbol{\sigma}d\Gamma = 0. \quad (6)$$

Here $\boldsymbol{\sigma}$ is the Cauchy stress tensor for a linear elastic body defined as

$$\boldsymbol{\sigma} = \mu\nabla\mathbf{d} + \mu\nabla\mathbf{d}^T + \lambda\mathrm{tr}(\nabla\mathbf{d})\mathbf{I}, \quad (7)$$

where $\mathbf{d}$ is the total displacement vector, μ and λ are the Lamé coefficients defined in terms of the Young's modulus of elasticity, E_s, and Poisson's ratio, ν_s, as:

$$\mu = \frac{E_s}{2(1+\nu_s)}, \quad (8)$$

$$\lambda = \frac{\nu_s E_s}{(1+\nu_s)(1-\nu_s)}. \quad (9)$$

2.2.1. Block-Coupled Procedure

The block-coupled numerical solution for linear elasticity and unstructured meshes is used to solve the structural model [11]. This numerical procedure differs from the more commonly used segregated approach, where each dimension is solved separately, in that the inter-component coupling is implicitly included as coefficients within a block matrix [11]. In benchmark tests against segregated approaches, Cardiff et al. [11] demonstrated significant clock time reduction for both 2-D and 3-D test cases, although this comes at the price of increased memory requirements. Based on the recommendations from these benchmark tests, a direct linear solver (`EigenSparseLU`) based on LU Decomposition method is applied here since it was shown to be the most computational efficient for 2-D cases [11], which are the focus of this study.

2.3. Fluid-Structure Domain Coupling

Each region has an independent mesh on which the corresponding governing equations are applied. For the solid, the deformation field, $\mathbf{d}$, is solved on a static mesh using the projected tractive forces from the fluid domain as the boundary conditions. The calculated interface forces are transferred back to the fluid domain, and the mesh is deformed based on the projected structural displacements at each time step. The updated mesh is calculated using the cell-centre Laplacian for the motion velocity based on an inverse distance quadratic diffusivity relative to the structure's instantaneous position.

The fluid and structure domains are strongly-coupled via an iterative Dirichlet-Neumann algorithm [61]. This approach involves the application of a Dirichlet condition in the fluid domain for the velocity at the interface between the two regions, whilst utilising a Neumann condition for

Algorithm 1 FSI Coupling Procedure [8]

while time < end time **do**
1. Start next time step
2. Estimate initial interface residual.
while residual > ϵ and iteration < i_{max} **do**
3. Switch to the next iteration.
4. Calculate the interface displacements in the fluid domain.
5. Solve the mesh motion equation.
6. Update the fluid mesh.
7. Solve the fluid governing equations.
8. Project the interface forces from the fluid to solid domain.
9. Solve the structural governing equations.
10. Project the interface displacements from the solid to the fluid domain.
11. Calculate interface residual in fluid domain.
end while
end while

Parameter	Notation	Value
Under-Relaxation Method		Aitken
Residual Tolerance	ϵ	1×10^{-5}
Max Iterations	i_{max}	30
Initial relaxation	ω_0	0.25

Table 1: Coupling parameter values used in this study.

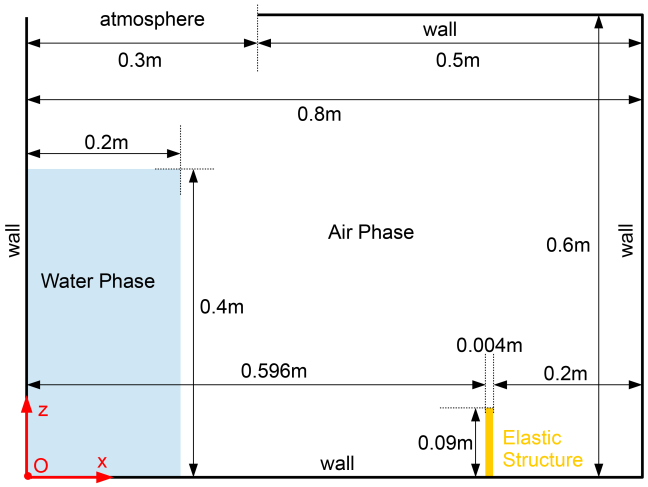

Figure 1: Diagram of the numerical setup for the dam break test case.

traction at the interface in the solid domain [8]. A maximum of $i_{max} = 30$ inner loop iterations are applied to achieve the strong-coupling, which ensures that the mesh deformation is consistent with the kinematic and dynamic conditions at the interface at each time step. The termination criterion for the inner loop iterations is a user-specified relative residual for the interface displacement, set to $\epsilon = 1 \times 10^{-5}$ in this work. Dynamic Aitken under-relaxation [2, 26] is used to accelerate convergence of the coupling algorithm, which adapts the under-relaxation factor in each inner loop iteration based on the present residuals of the data. The initial under-relaxation factor is set to $\omega_0 = 0.25$ in this work. A summary of the coupling procedure is presented in Algorithm 1 with the coupling parameters utilised in this study provided in Table 1.

3. Dam Break on Flexible Structures

In this section, the proposed numerical approach and setup is validated against a dam break interaction with an elastic structure. This problem is selected since dam break scenarios are common numerical benchmarks for two-phase flows, and consequently have similarities with wave-driven hydroelastic impacts which are the primary focus of this work (Section 4). Furthermore physical data is available [35] for the proposed test case and previous numerical solutions have been published [35, 40], strengthening the validation.

3.1. Numerical Setup

A quasi 2-D numerical domain of length 0.8 m and height 0.6 m is utilised to be consistent with the water tank from the experiments [35]. The coordinate system is defined such that x and z are the horizontal and vertical components, respectively, with the origin located at the bottom left hand corner of the domain. All of the boundaries are considered to be walls with no slip conditions applied with the exception of the top boundary which is split into two regions: a wall boundary for $x \geq 0.3$ m where no slip conditions are applied; and an atmospheric boundary for $x < 0.3$ m (representing an open region in the experiments used to remove the containing gate) where a non-reflecting pressure boundary condition is utilised to allow air to leave or enter the domain. Based on the results of a mesh independence study (Section 3.1.1), the domain is discretised with a $\Delta x_f = \Delta z_f = 0.002$ m resolution throughout, creating a total fluid mesh size of 119910 cells.

A thin flexible structure of height 0.09 m and thickness 0.004 m is installed in a vertical orientation with a fixed boundary on the bottom wall of the water tank (Figure 1). The structural domain is discretised using $\Delta x_s = 0.0002$ m and $\Delta z_s = 0.002$ m, creating a total mesh size of 900 cells. The structure is considered to be constructed from natural rubber of density $\rho_s = 1161.54\,\text{kg}\cdot\text{m}^{-3}$, Poisson's ratio $\nu_s = 0.49$ and Young's modulus $E_s = 3.5\times10^6$ Pa. The structure is modelled as a moving wall boundary in the fluid domain, which applies no-slip conditions whilst accounting for the motion of the wall, and zero-traction for the solid domain.

The fluid is modelled as a two-phase continuum using the VOF method with the properties of air and water at temperatures of $T = 25\,^\circ$C, as detailed by Liao et al. [35]. A water column of height 0.4 m and width 0.2 m is located against the left wall of the water tank, and initially (at time $t = 0$ s) the fluid is considered to be still. In the experimental campaign, the fluid was contained by a vertical gate which was raised at $t = 0$ s [35] but, for simplicity, this gate is not modelled in the present numerical study and instead the fluid column is released under gravity at $t = 0$ s. A variable small step is utilised based on a maximum Courant number of 0.5, with an additional constraint imposed that the maximum time step is 0.0001 s. This is found to improve numerical stability due to the explicit nature of the coupling between the phase function indicator problem, the momentum prediction and the pressure correction step.

3.1.1. Mesh Independence Study

Due to the coupled nature of the problem, a mesh independence study is conducted using a multi-step process by considering the discretisation of the fluid and solid domain individually whilst fixing the cell size in the other.

Firstly, the vertical discretisation in the solid domain (Δz_s) is considered, whilst fixing the fluid resolution ($\Delta x_f = \Delta z_f = 4$ mm). A significant difference in the solution between $\Delta z_s = 4$ mm and $\Delta z_s = 2$ mm is observed (Figure 2a),

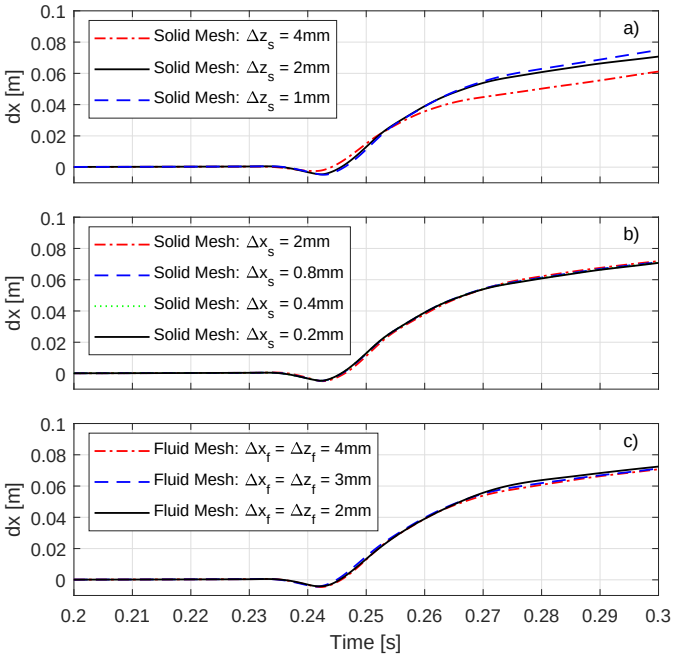

Figure 2: Mesh independence study for the solid domain vertical resolution (a), solid domain horizontal resolution (b) and fluid domain (c). The horizontal displacement at Marker 1 (z = 0.0875) is presented. In each case, the other two discretisations are fixed: $\Delta x_f = \Delta z_f = 4$ mm for the fluid domain (a,b); $\Delta z_s = 2$ mm for the vertical solid domain (b,c); and $\Delta x_s = 0.2$ mm for the horizontal solid domain (a,c).

and another smaller discrepancy between $\Delta z_s = 2$ mm and $\Delta z_s = 1$ mm. Although this indicates that the mesh is not fully converged, the $\Delta z_s = 1$ mm simulation is less robust, thought to be due to the discrepancy with fluid discretisation. Therefore, $\Delta z_s = 1$ mm is utilised in this study for the vertical resolution in the solid domain, which is consistent with previous studies [40].

Secondly, the solid domain horizontal resolution (Δx_s) is tested by fixing the fluid ($\Delta x_f = \Delta z_f = 4$ mm) and vertical solid ($\Delta z_s = 2$ mm) cell sizes, and varying the horizontal discretisation. The results imply that the solution is not overly sensitive to the horizontal solid resolution, and that for less than $\Delta x = 0.8$ mm the case is converged (Figure 2b). A discretisation of $\Delta x = 0.2$ mm is selected for this study.

Finally, the fluid discretisation ($\Delta x_f = \Delta z_f$) is varied, whilst using the aforementioned solid discretisation ($\Delta x_s = 0.2$ mm, $\Delta z_s = 2$ mm). There are minor discrepancies between the three mesh resolutions tested (Figure 2c), but the magnitude is generally quite similar. However, the $\Delta x_f = \Delta z_f = 2$ mm resolution is selected to match the vertical discretisation in the solid domain, and hence minimise the interpolation error.

3.2. Results

Figure 3 presents time series comparisons of the horizontal displacement, dx, for the numerical model (——) and experimental data (□) [35]. Data from the three marker locations tracked in the experimental campaign [35] are presented, which at $t = 0$ s are located at the centreline of the structure ($x = 0.598$ m) and at $z = 0.0875$ m (Marker 1), $z = 0.065$ m (Marker 2), and $z = 0.04$ m (Marker 3). Also plotted are previous numerical solutions from Liao et al. [35] (– – –) and, for Marker 1 only, Martínez-Ferrer et al. [40] (– · –). Comparing the results at Marker 1 (Figure 3a), it is observed that the present model overestimates the displacement of the structure at the tip of the structure relative to the physical data, particularly at the peak response. The previous numerical solutions show slightly improved agreement with the peak displacement, although Martínez-Ferrer et al. [40] exhibits similar discrepancies as the present model otherwise. At Markers 2 and 3 the agreement between the present model and the experiments is significantly improved, and is consistent with the discrepancies of Liao et al. [35].

Comparing spatial snapshots of the present numerical model solutions with photographs from the experiments (Figure 4), it is observed that for the relatively small deformations in the frames soon after the impact ($t - t_i \leq 0.025$ s), the agreement is good. However, in later frames ($t - t_i > 0.025$ s), there are greater discrepancies. In the numerical model, the structure overturns to a lesser degree and instead appears to stretch, and consequently causes an over-estimate in peak horizontal displacement for Marker 1 (Figure 3a). This discrepancy is thought to be due to the use of a linear elastic model, which is less accurate for the large deformations observed in these

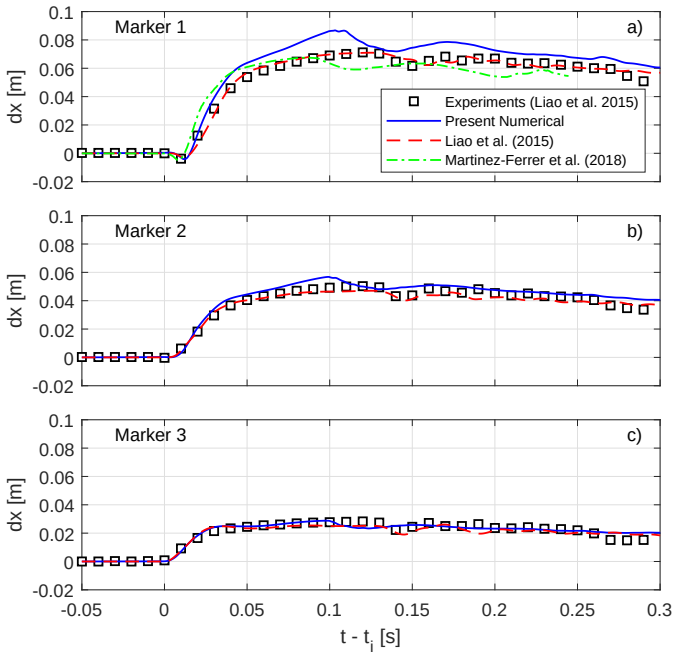

Figure 3: Predicted horizontal displacement time series' (——) compared with physical data [35] (□). Time is relative to the first impact on the structure, t_i. Three points are presented located at $x = 0.598$ m, and: $z = 0.0875$ m (Marker 1; a); $z = 0.065$ m (Marker 2; b); and $z = 0.04$ m (Marker 3; c). Previous numerical solutions from [35] (– – –) and [40] (– · –) are also presented.

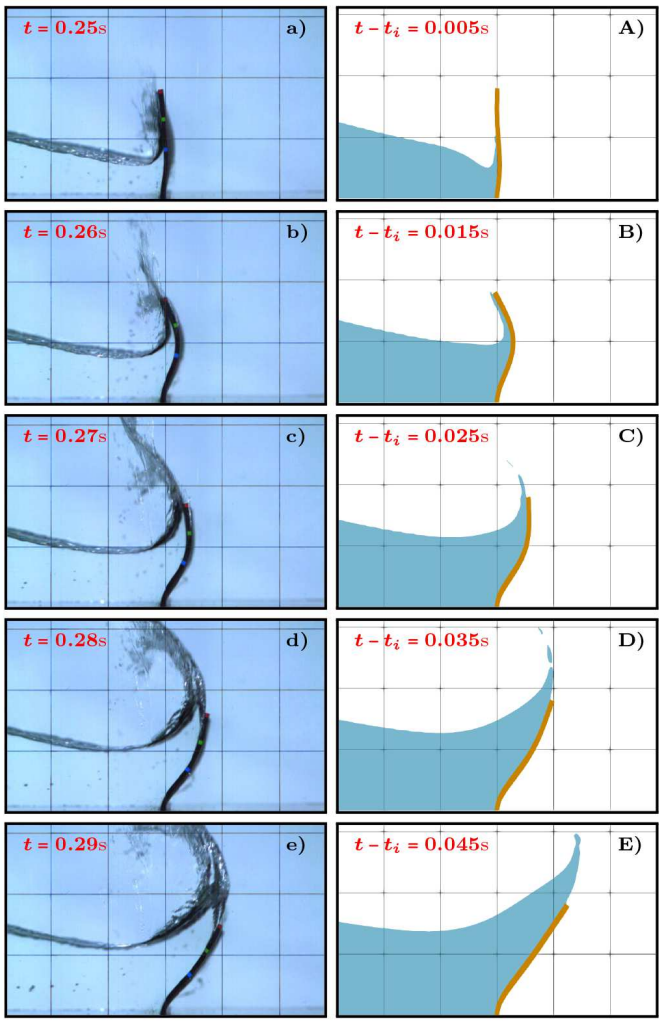

Figure 4: Instantaneous snapshots of the structure's deformation in the experiments of Liao et al. [35] (a-e) and numerical model (A-E). The grid resolution is 5 cm.

frames. This is consistent with the previous numerical solutions, which utilised non-linear elastic models [34, 40] and demonstrated the ability to capture peak deformation. The primary aim of this work, however, is to investigate hydroelastic interactions for floating structures in monochromatic waves, for which it is anticipated that the deformations will be significantly less than observed in this case. Since the model performed well when the deformations are relatively small (lower in the structure as well as in the early frames) and agreed with previous numerical models, it is considered to be sufficiently validated for the present application. Future work, however, should focus on alternative solid solvers to improve results for the large deformations that may occur in more general wave-driven hydroelastic applications.

4. Wave Interaction with Floating Structures

The numerical model, validated against experimental and numerical data for two-phase flows in Section 3, is used here to investigate monochromatic wave interactions with elastic structures of varying dimensions. Novel physical data obtained from an experimental campaign in the Coastal, Ocean And Sediment Transport (COAST) Laboratory at the University of Plymouth is presented for comparison. In this section the coordinate system is defined such that x and z are the horizontal and vertical components, respectively, with the origin located at upstream edge of the structure and at the still water level (Figure 6).

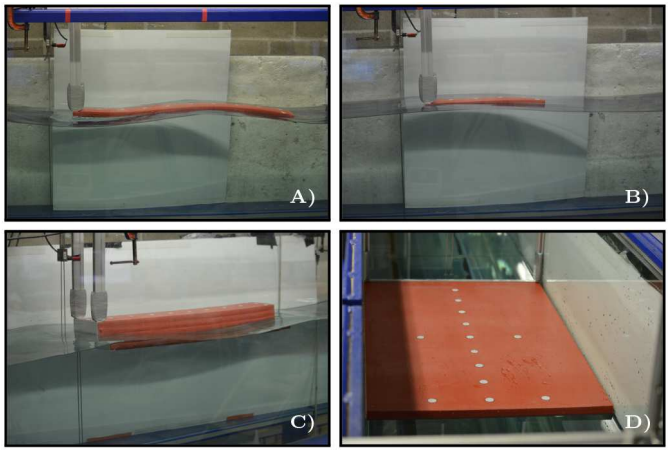

Figure 5: Photographs of the wave-driven hydroelasticity experimental setup in the COAST Laboratory, University of Plymouth, UK.

4.1. Experimental Setup

Experiments are conducted in the sediment wave flume at the COAST Laboratory, using flexible floating structures of varying dimensions (Table 2; Figure 5) constructed from silicone sponge with properties $E_s = 5.65 \times 10^5$ Pa and $\nu_s = 0.49$. The density of each structure is approximately $\rho_s = 380\,\mathrm{kg/m^3}$ but varies slightly between structures (see Table 2). The structures are tested in regular waves of period $T = 1.04$ s and amplitude $a = 0.009$ m, generated using an energy absorbing piston-type paddle in a water depth of 0.75 m. An absorbing beach is installed at the end of the wave flume to minimise wave reflections

Station-keeping is an important consideration in laboratory testing of floating structures in general, but it is crucial in hydroelastic modelling since it can have such a large influence on the structural response and is applica-

Structure	Length m	Width m	Height m	Density kg/m^3
A	0.960	0.146	0.025	369
B	0.483	0.146	0.025	362
C	0.953	0.147	0.100	388
D	0.961	0.595	0.025	412

Table 2: Dimensions and density of the deformable structures constructed from silicone sponge assessed in the COAST Laboratory's wave flume.

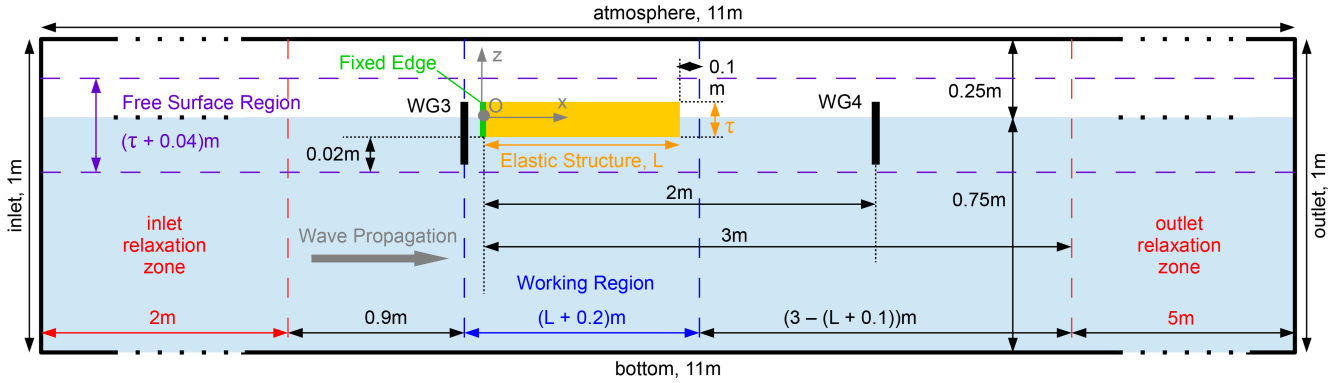

Figure 6: Diagram of the numerical domain. Note that although the domain dimensions are the same in all cases, the working region and free surface zone are defined relative to the structure's length, L and thickness τ, respectively.

tion specific. Therefore, a variety of constraining methodologies have been demonstrated in the literature: Sendil and Graf [53] used chain moorings attached to the sea bed for experiments motivated by floating breakwaters; Bennetts et al. [4] utilised a compliant four-point mooring system, minimising the effect on the ice floe model but not allowing for free drift; Montiel et al. [42] deployed a two vertical rod approach to constrain surge, sway and yaw of floating discs; Sree et al. [54] demonstrated a stopper rod on the downstream edge to constrain surge, while having negligible effect on the deformation of the ice model. In this work, however, each structure is installed in the 35 m × 0.6 m wave flume such that the upstream edge is constrained at the vertical equilibrium location, using a top mounted approach to minimise the influence on the hydrodynamics. The remainder of the structure is floating and free to deform (Figure 5), creating a similar scenario to a simplified attenuator type WEC.

Measurement of the response is one of the key challenges in physical modelling of single-piece homogeneous structures since instruments cannot be easily implemented within the material. In this work, the structure's deformation is tracked using a non-contact Qualysis motion capture system, providing the instantaneous position of fixed markers located on the top edge of each structure at a sampling rate of 128 Hz. To minimise reflection off the glass side walls and free surface, the infrared LED cameras are positioned at an angle above the open-topped wave flume, focusing on the top of the structure. The system is calibrated relative to a fixed point on the bottom of the flume, with a typical residual in the range of 0.5 – 1 mm. In this study, the problem is considered to be described by a 2-D slice in the $x - z$ plane and hence all comparisons are relative to data from the centreline of the structure ($y = 0$ m), on which Qualysis markers are placed at 0.1 m intervals, unless stated otherwise. To record the free surface elevation four resistance wave gauges are installed at: $x = -3.6$ m (WG1); $x = -2.6$ m (WG2); $x = -0.1$ m (WG3); and $x = 2$ m (WG4). Once calibrated, the wave gauges have an associated error of less than 0.36%.

4.2. Numerical Setup

The quasi 2-D numerical domain is setup to represent a $x - z$ plane slice of the physical wave tank, reduced to 11m in length for computational efficiency, and 1 m in height with a water depth of 0.75 m (Figure 6). The deformable structure is fixed on its upstream boundary, located at $x = 0$ m, but otherwise is considered to be flexible, i.e. free to deform due to the interaction with the wave. In the vertical dimension, the fixed boundary is situated at the equilibrium position of the structure in still water, which is initially set as a flat (undeformed) horizontal rectangle (Figure 6).

The numerical domain for the fluid component of the model is designed such that there is a working region in

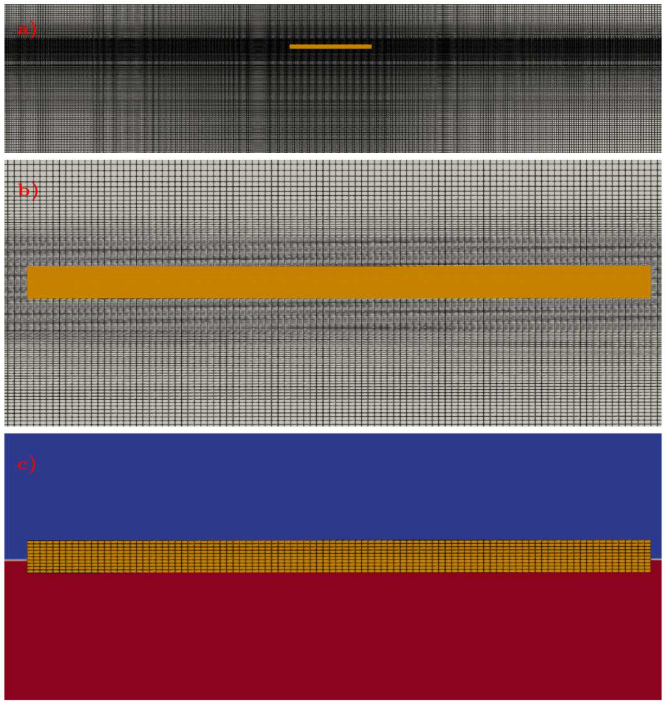

Figure 7: The mesh structure used for the fluid domain (a and b) and the solid domain (c).

the horizontal dimension defined as the region bounded by 0.1 m at either end of the structure (Figure 6). In the vertical dimension there is a free surface region which is considered to be the region bounded by 0.02 m above and below the position of the structure at equilibrium. Based on an initial mesh independence study without the structure present, a uniform horizontal discretisation of $\Delta x_f = 0.005$ m is used in the working region, with horizontal mesh grading utilised towards the inlet/outlet boundaries to minimise the computational effort. In preliminary simulations, it was noted that the deformation of the structure is sensitive to the vertical resolution in the free surface region even in still water conditions. This is thought to be due to a combination of interpolation between the two domains and the smearing of the interface in the VOF scheme and, hence, the vertical resolution is set to be finer ($\Delta z_f = 0.001$ m) than the horizontal discretisation in the free surface region to minimise this dependency (Figure 7). The vertical free surface resolution results in 18 cells per wave height, which should resolve the wave within a RMS tolerance of 1% [47]. Outside of the free surface region, vertical mesh grading is used towards the atmosphere and bottom boundaries.

For the structural domain, the horizontal resolution is $\Delta x_s = 0.005$ m and is coincident to the fluid domain to minimise interpolation error. In the vertical dimension, a resolution of $\Delta z_s = 0.0025$ m is applied based on the results of an initial mesh independence study for structure B in monochromatic waves. The final fluid and solid meshes vary due to the different dimensions of the structure but have approximately 180000 and 2000 cells, respectively.

The two phases of the VOF method are set to the properties of air ($\rho_0 = 1.22\,\mathrm{kg/m^3}$, $\nu_0 = 1.48 \times 10^{-5}$ Pa/s) and fresh water ($\rho_1 = 1000\,\mathrm{kg/m^3}$, $\nu_1 = 1 \times 10^{-6}$ Pa/s), respectively. The initial conditions for the fluid correspond to still water. Wave generation is achieved at the inlet boundary via Stoke's second order [55] expression-based boundary conditions. Relaxation zones provided through the `waves2Foam` toolbox [28], are utilised at the inlet and outlet boundaries to improve the quality of the wave generation and minimise reflections. Previous studies have shown that an inlet relaxation zone of length greater than a wavelength, l, is suitable for capturing the wave profile [5] and hence it is set to 2 m ($\geq 1.2l$) in this work. The outlet relaxation zone has a target solution of still water and is 5 m in length ($\geq 3l$) which will correspond to a reflection coefficient of $R < 0.001$ [28]. The remaining boundary conditions are: non-slip conditions for the bottom boundary; total pressure for the atmosphere; a zero displacement on the fixed edge of structure; and a zero-traction condition on the deformable boundaries of the structure. The simulations are run with an adjustable timestep based on a maximum Courant condition of $Co = 0.5$, but with an additional constraint on the maximum time step ($\Delta t < 0.001$ s) to ensure numerical stability.

Note that the phases are defined such that the numerical solution and experimental data are in-phase at the second Qualysis marker (at $x = 0.115$ m), with the peak occurring at $t/T = 0$. This point is selected since it is the closest point to the fixed end which has a clear maxima in all cases, and the convention is used consistently throughout this section.

4.3. Results

Figure 8 presents a spatial comparison of the predicted numerical solutions (line) and experimental data (circles) for the four different structures at varying wave phase. The vertical displacement, dz, is plotted as a function of x/L, where L is the length of the structure. The numerical predictions for structures A (Figures 8Aa - 8Aj) and D (Figures 8Da - 8Dj) are generally in good agreement with the physical data, although the magnitude of the vertical displacement is underestimated near the middle ($0.4 < x/L < 0.8$) of structure A, particularly when this section is near its minima (Figures 8Ag - 8Ai). The predicted qualitative behaviour of structures B and C is in reasonable agreement with the experiments but the magnitude of the vertical displacement is generally under-predicted towards the free end ($x/L > 0.5$). This under-estimation could be partly explained by numerical diffusion, although mesh-related diffusion has been minimised through a thorough mesh independence study. Another possible explanation is that, although the problem is thought to be dominated by Froude scaling, viscous effects may be non-negligible and hence the agreement may be improved through use of a turbulence closure model. The magnitude of response for structure D, however, is captured well by the model, and this inconsistency with the results for the other structures implies that both numerical diffusion and turbulent effects are not the primary cause of the discrepancy. It is hence hypothesised that 3-D effects may be non-negligible since structure D is the only model that spans the full width of the flume, and its response is captured best by the present 2-D numerical approach. The potential 3-D effects are discussed in more detail later in this section. Inclusion of turbulent effects, however, could potentially still improve the results near the free end of the structure, and more generally, will be a key consideration in many wave-driven hydroelastic interactions with higher non-linearities. Hence, turbulence closure models will be investigated as part of future work.

Figure 9 presents the horizontal-vertical displacement paths from 5 wave cycles of each structure focusing on the markers located at: $x/L \approx 0.224$ (blue); $x/L \approx 0.432$ (red); $x/L \approx 0.641$ (yellow); and $x/L \approx 0.953$ (purple). There is generally quite low variation in the path of each marker over successive wave cycles, showing a quasi-steady state has been reached in both the experiments and the numerical model, with the exception of the marker located at $x/L = 0.641$ on structure C (which deviated on one cycle). Focusing purely on the experimental profiles (Figures 9a,c,e,g), it is observed that for structure A the magnitude of the vertical displacement is similar for all points

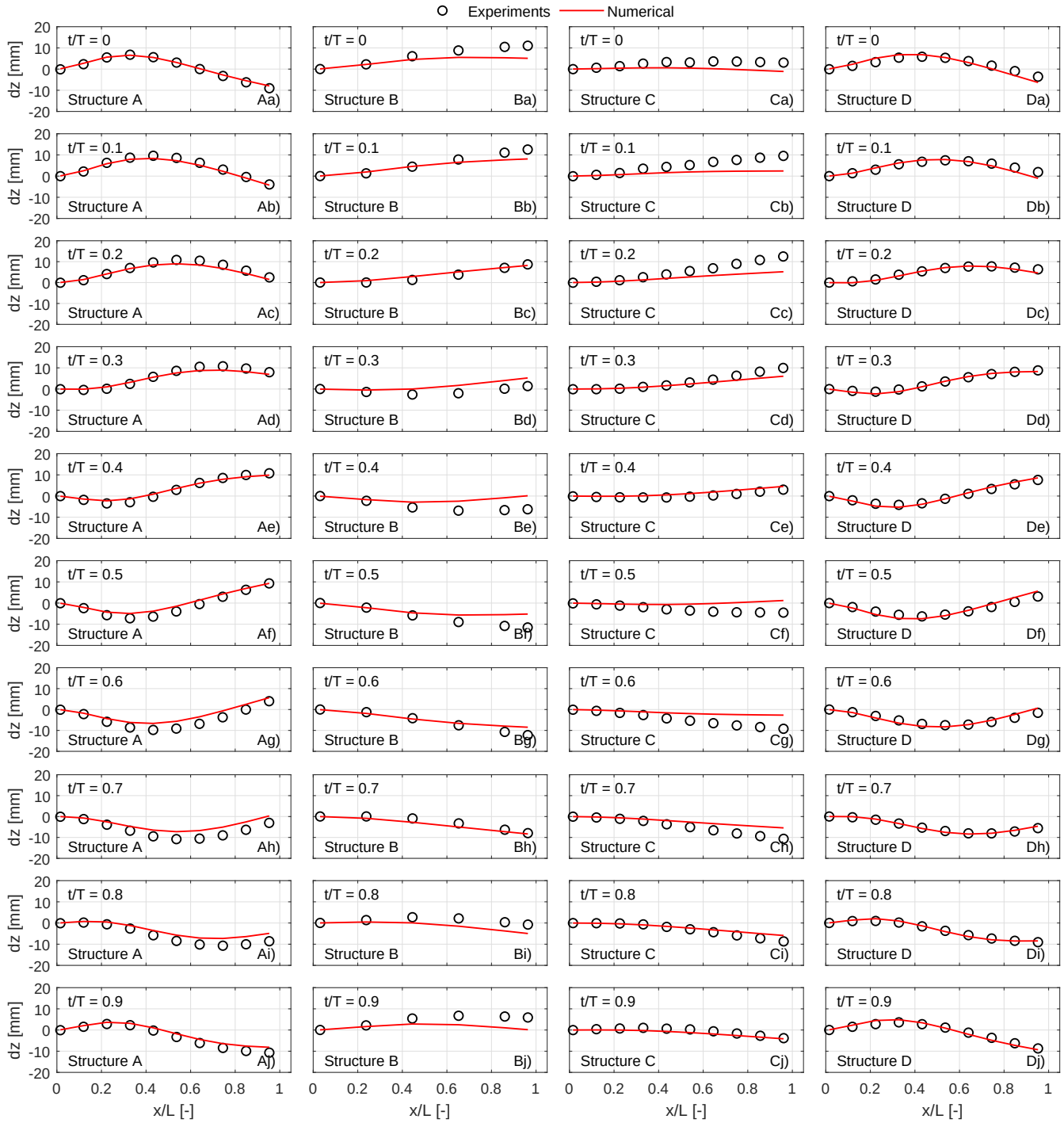

Figure 8: Numerical prediction (—) of vertical displacement, dz, as a function x normalised by the structure's length, L, compared with experimental data (∘). Wave phases are plotted on the rows (a-j), with the four columns representing the different structures': structure A (Aa-Aj); structure B (Ba-Bj); structure C (Ca-Cj); and structure D (Da-Dj).

greater than x/L = 0.432. The profiles for structures B and C, on the other hand, exhibit a progressive increase in vertical displacement with distance from the fixed edge. Structure B is significantly shorter than structure A (Table 2), and consequently x/L = 0.432 is located considerably closer to the fixed edge in terms of absolute distance. Hence, it is likely that there is more influence from this fixing, accounting for this reduced magnitude compared with structure A, which would be relatively less constrained. Structure C is significantly thicker than structure A (Table 2), leading to increased bending resistance and hence the material bends less closer to the fixed edge. Considering the magnitude of the horizontal displacements, it is noted that it remains similar for each of the four sampling points for cases A, B and D, indicating consistent stretch along the length of the structure. Structure C, however,

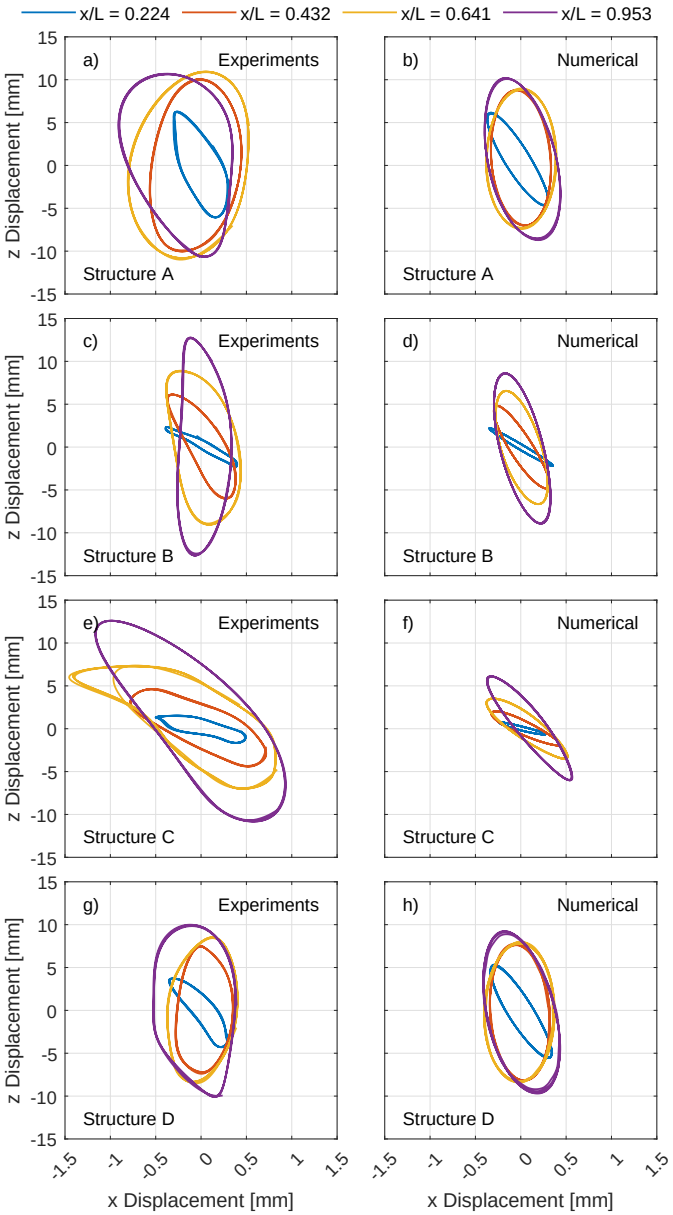

Figure 9: Deformation paths ($dx - dz$) taken by four different markers on the structure in the experiments (a,c,e,g) and the equivalent predictions from the numerical model (b,d,f,h). Each row represents a different structure: structure A (a,b); structure B (c,d); structure C (e,f); and structure D (g,h). Note that the length scales in x and z are different.

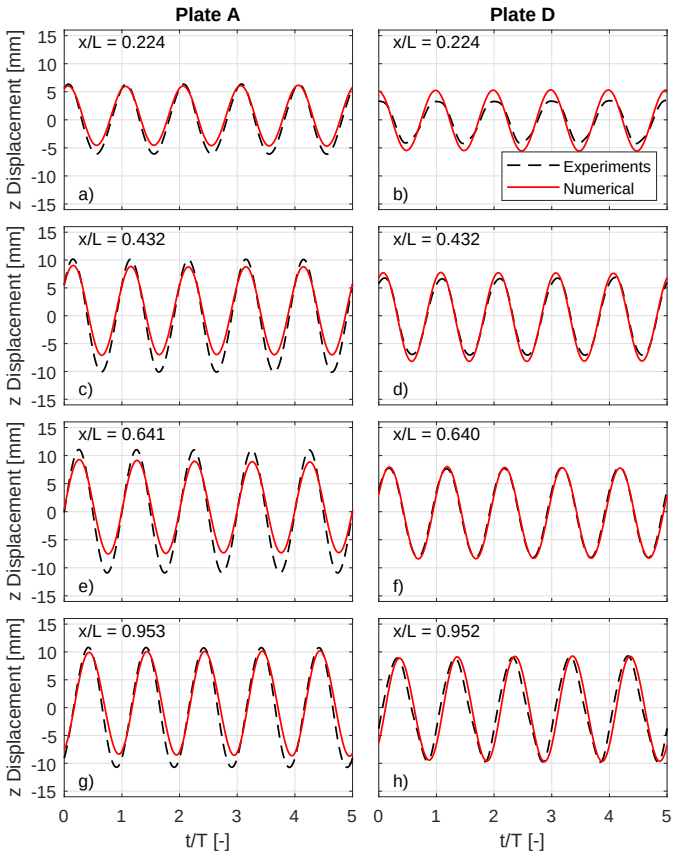

Figure 10: Time series' comparison of experimental (– – –) and numerical (——) data for structures A and D. The time axis has been normalised by wave period ($T = 1.04\,\mathrm{s}$).

exhibits a progressive increase in horizontal displacement along the structure. Since this structure has a greater thickness than the others, this is thought to be due to the increased bending resistance which in turn leads to an increase in stretching instead.

The numerically predicted behaviour (Figures 9b,d,f,h), is generally in qualitative agreement with the physical data, exhibiting flatter orbits for structure C and points close to the fixed end of the structure. However, as noted in Figure 8 the magnitude is underestimated, particularly for $x/L > 0.5$ in structures B and C. Furthermore, the paths generally tend to be close to an elliptical orbit in the numerical model, which is not necessarily observed in the physical data, particularly near the unconstrained end of the structure (see $x/L = 0.953$ for all structures). This may indicate that in the experiments additional modes are being excited which are not being captured well by the present numerical approach. This could potentially be due to the properties of the silicone sponge not being perfectly uniform, or alternatively the use of a linear structural model. Therefore, the effect of utilising a non-linear modelling approach for the structural mechanics will be explored in the future.

The results for structures A and D are particularly interesting since the length and thickness of the structures are very similar and yet the magnitudes of the vertical deformation differ (Figures 8 and 9). Comparing time series' of the responses (Figure 10) it is observed that the numerical solution is similar for both structures. This is to be expected since the problem is modelled in 2-D and only differs in length by 1 mm and in density, a parameter which preliminary simulations showed the model is not overly sensitive towards. However, in the experiments there are much greater differences in the response of these structures, with larger deformations occurring in structure A. Since the most significant difference between the two

	Structure			
	A	B	C	D
Physical	0.8024	0.8372	0.8231	0.5556
Numerical	0.6827	0.6670	0.3883	0.6827

Table 3: Numerical and physical downstream (WG4) to upstream (WG3) wave height ratio for structures A-D.

cases is the width of the structure (Table 2), it is thought that 3-D effects or blockage are the primary cause of the discrepancy. In particular, there is a significant reduction in downstream wave height for structure D in the experiments (Table 3), indicating greater wave reflection or absorption from this structure. In the numerical model, the downstream wave height reduction is consistent for structures A and D (Table 3) which, as noted previously, is to be expected since they are both modelled in 2-D, i.e. as an infinitely wide floating structure. This approach is most representative of structure D, which is in-line with the better agreement with the experimental data observed for this case in Figures 8 and 9.

Comparing the wave gauge data for structures A-C, none of which span the full width of the wave flume, it is observed that there is significantly larger wave reflection or absorption due to the structure in the numerical model compared to the experiments. This could partially explain the under-predictions in deformation seen in Figures 8 and 9. Structure C exhibits particular large under-predictions in deformation and also has the largest reduction in downstream wave height compared with the experiments (Table 3). The greater thickness of this structure considerably increases the blockage of the water column (and consequently the wave reflection and absorption), and hence any inaccuracies associated with modelling this scenario in 2-D are amplified. At present, although the `solids4foam` toolbox does allow for fully 3-D simulations it is infeasible to extend the present setup due to the extremely high computational cost. Even with the relatively modest number of cells used in the present simulation (180k for fluid mesh; 2k for solid mesh), every 1 s of simulation time typically requires 36 hours of clock time (on a single 3.4 GHz core). High computational cost should be expected for any FSI simulation due to a combination of iterative procedures required to achieve a strong coupling and a small time step to ensure numerical stability. Hence, in the future, parallel computing could help to improve the overall time taken to produce a result but this is not presently implemented for the direct linear matrix solver used in this work. It is worth noting that in preliminary simulations, utilising similar mesh sizes as presented in this work, the computational efficiency observed for the block-coupled approach was considerably better than alternative methods within the numerical toolbox that were run in parallel. Recent advancements in the toolbox include a modified block-coupled scheme [9] that has been demonstrated to be parallelisable, and any improvements in computational cost offered by this functionality will be investigated as part of future work.

Furthermore, future effort will aim to optimise the problem in order to make the application of the present code more practical. The computational cost is always going to be large for this type of problem due to the necessity of a strongly-coupled iterative algorithm, and relatively small timestep. It is therefore essential that both the domain size, mesh resolution and total simulation time are minimised. The present setup suffers from additional considerations that need optimising: a long domain (multiple wavelengths) in order to accurately resolve the wave; fine mesh resolution around the free surface to accurately capture the interface and interpolation to the structure; and increased simulation time to allow for wave propagation. It may be that the present problem would be ideally suited towards a multi-region approach [39], where the present numerical model is only applied in a small region in the immediate vicinity of the structure, and the propagating wave is resolved in a separate larger region with a lower-order hydrodynamic solver.

5. Conclusions

Motivated by offshore renewable energy applications, the aim of this study is to provide novel experimental data to assist with the development of coupled numerical tools for simulating fully nonlinear hydroelastic interactions with highly-flexible floating structures. Numerical results are presented for comparison, obtained using the `solids4Foam` toolbox which is a collection of solvers and libraries of varying fidelity for generalised 3-D FSI simulations. The presented numerical model, however, is limited to a 2-D partitioned approach consisting of a two-phase fluid flow modelled using the VOF method and modified for relaxation zones; a linear solid model for small deformations solved via the block-coupled method [11]; and strong-coupling through the Dirichlet-Neumann approach with dynamic Aitken under-relaxation. The numerical model is validated against a representative dam break benchmark, and is shown to perform well relative to experimental data and previous numerical solutions, although the extension of the structure for large deformations is over-predicted. Future effort, therefore, will be aimed at identifying a solid model for more general wave-driven hydroelastic applications that include large deformations, through exploration of alternative approaches available within the numerical toolbox.

In monochromatic wave interactions with highly-flexible floating structures, the numerical predictions are in reasonable agreement with the data from the novel physical modelling campaign conducted in the COAST Laboratory at the University of Plymouth. Considering structures of varying dimensions (length and thickness) with a fixed width (small relative to physical tank's width), the numerical model showed consistent qualitative agreement with

the experiments in that the larger deformations occurred in the thinner structures. However, the magnitude of the deformation is consistently under-estimated. Comparison of downstream and upstream wave heights indicated that there is significantly larger wave reflection and/or absorption in the numerical model, indicating that a 3-D approach may be necessary in order to capture the magnitude of these structure's motion more accurately. Comparison with experimental data for a structure approximately the width of the wave tank backs up this conclusion, since the agreement is much improved. Future work will focus on assessing variations in material properties, different attachment configurations and the effect of wave period through both further physical and numerical modelling.

Overall, the results indicate that the numerical code has good potential for future application to wave-driven hydroelastic problems, especially scenarios which can be reduced to a 2-D setup. Future work will focus on providing further experimental data for more complex hydrodynamic conditions; alternative materials with varying stiffness; different station-keeping methods; and scenarios which exhibit clear 3-D effects. Extending the numerical simulations to 3-D is clearly desirable in the future, and although the `solids4foam` toolbox presently contains the functionality to achieve this, the prohibitive computational cost observed in this work makes this transition non-trivial. Due to the iterative procedures involved in the strong-coupling, the computational cost is always going to be high for FSI applications but this can be offset in many instances by minimising the size of the problem (both spatially and temporally). However, in wave-driven hydroelasticity applications additional constraints make it difficult to achieve this minimisation, such as the requirement to resolve several wavelengths and hence wave periods. Hence, optimisation of the numerical approach is required if the code is to be of practical use in these applications. Potential methods to achieve this are to assess alternative methods within `solids4foam`, including those which allow for parallelisation; integrate the method within a hierarchical modelling approach where the FSI only acts in a small region (directly surrounding the structure) of the overall problem; and/or make compromises surrounding the mesh resolution and consequent quality of the wave. This optimisation will be the focus of future work.

Acknowledgements

The authors gratefully acknowledge that this work was funded by the Engineering and Physical Sciences Research Council primarily through 'A zonal CFD approach for fully nonlinear simulations of two vessels in launch and recovery operations' [EP/N008847/1], with additional support from the 'Partnership for Research in Marine Renewable Energy' [EP/P026109/1] and 'Supergen ORE Hub' [EP/S000747/1]. The authors would like to thank Dr. Zheng Zheng Hu for her valuable support on project EP/N008847/1. The experimental data presented in this work is made publicly available via a test case for 'A Collaborative Computational Project in Wave Structure Interaction' [EP/T026782/1].

References

[1] Aghaei, A., Schimmels, S., Schlurmann, T., Hildebrandt, A., . Numerical investigation of the effect of aeration and hydroelasticity on impact loading and structural response for elastic plates during water entry. Ocean Engineering 201.

[2] Aitken, A., 1926. On Bernoulli's numerical solution of algebraic equations. Proceedings of the Royal Society of Edinburgh 46, 289–305.

[3] Bathe, K.J., Ramm, E., E.L., W., 1975. Finite element formulations for large deformation dynamic analysis. International Journal for Numerical Methods in Engineering 9, 353–386.

[4] Bennetts, L., Alberello, A., Meylan, M., Cavaliere, C., Babanin, A.V.and Toffolli, A., . An idealised experimental model of ocean surface wave transmission by an ice floe. Ocean Modelling 96, 85–92.

[5] Brown, S., Greaves, D., Magar, V., Conley, D., 2016. Evaluation of turbulence closure models under spilling and plunging breakers in the surf zone. Coast. Eng. 114, 177–193.

[6] Brown, S., Musiedlak, P.H., Ransley, E., Greaves, D., 2019. Quantifying the predictive capability of OpenFOAM 4.1: Focused wave interactions with a fixed FPSO. International Journal of Offshore and Polar Engineering 29, 158–164.

[7] Brown, S., Musiedlak, P.H., Ransley, E., Greaves, D., 2020. Quantifying the predictive capability of OpenFOAM 5.0: Focused wave impacts with floating bodies. International Journal of Offshore and Polar Engineering 30, 20–27.

[8] Cardiff, P., 2019. Solid mechanics and fluid-solid interaction using the solids4foam toolbox, in: 14th OpenFOAM Workshop, Duisburg, Germany.

[9] Cardiff, P., 2022. solids4foam overview and future directions. doi:10.13140/RG.2.2.17145.54883. presented at 2nd CCP-WSI Hackathon.

[10] Cardiff, P., Karač, A., De Haeger, P., Jasak, H., Nagy, J., Ivanković, A., Tuković, Ž., 2018. An open-source finite volume toolbox for solid mechanics and fluid-solid-interaction simulations. ArXiv Prepr ArXiv180810736.

[11] Cardiff, P., Tuković, Ž.and Jasak, H., Ivanković, A., 2016. A block-coupled Finite Volume methodology for linear elasticity and unstructured meshes. Computers and Structures 175, 100–122.

[12] Craig, M., Piro, D., Schambach, L., Mesa, J., Kring, D., Maki, K., 2015. A comparison of fully-coupled hydroelastic simulation methods to predict slam-induced whipping, in: Proceedings of the 7th Conference on Hydroelasticy in Marine Technology, Split, Croatia. pp. 575–590.

[13] Dai, J., Wang, C., Utsunomiya, T., Duan, W., 2018. Review of recent research and developments on floating breakwaters. Ocean Engineering 158, 132–151.

[14] Day, A., Babarit, A., Fontaine, A., He, Y.P., Kraskowski, M., Murai, M., Penesis, I., Salvatore, F., Shin, H.K., 2015. Hydrodynamic modelling of marine renewable energy devices: A state of the art review. Ocean Engineering 108, 46–69.

[15] Ertekin, R., Wang, S., Riggs, H., 1994. Hydroelastic response of a floating runway., in: Proceedings of the International Conference on Hydroelasticity in Marine Technology, Trondheim, Norway. pp. 389–400.

[16] Gavriilidis, I., Huang, Y., 2021. Finite element analysis of tidal turbine blade subject to impact loads from sea animals. Energies 14, 7208.

[17] Gingold, R., Monaghan, J., 1977. Smoothed particle hydrodynamics: theory and application to non-spherical stars. Monthly Notices of the Royal Astronomical Society 181, 375–389.

[18] Gotoh, H., Khayyer, A., Shimizu, Y., . Entirely Lagrangian meshfree computational methods for hydroelastic

fluid-structure interactions in ocean engineering - reliability, adaptivity and generality. Applied Ocean Research 115.

[19] Hartmann, M., Onorato, M., De Vita, F., Clauss, G., Ehlers, S., von Bock und Polach, F., Schmitz, L., Hoffmann, N., Klein, M., 2022. Hydroelastic potential flow solver suited for nonlinear wave dynamics in ice-covered waters. Ocean Engineering 259.

[20] He, K., Ni, B., Xu, X., Wei, H., Xue, Y., 2022. Numerical simulation on the breakup of an ice sheet induced by regular incident waves. Applied Ocean Research 120.

[21] Hu, Z., Mai, T., Greaves, D., Raby, A., 2017. Investigations of offshore breaking wave impacts on a large offshore structure. Journal of Fluids and Structures 75, 99–116.

[22] Huang, L., 2017. An opensource solver for wave-induced fsi problems. Proceedings of CFD with OpenSource Software.

[23] Huang, L., Ren, K., Li, M., Tuković, Ž., Cardiff, P., Thomas, G., 2019. Fluid-structure interaction of a large ice sheet in waves. Ocean Engineering 182, 102–111.

[24] Ibrahimbegovic, A., 2009. Nonlinear solid mechanics: Theoretical formulations and finite element solution methods. Springer.

[25] International Energy Agency, 2021. World Energy Balances: Overview. Technical Report. IEA. Paris. `https://www.iea.org/reports/world-energy-balances-overview`, Last Accessed: 23 Feb 2022.

[26] Irons, B., 1969. A version of the Aitken accelerator for computer iterations. International Journal of Numerical Methods in Engineering 1, 275–277.

[27] Issa, R.I., 1986. Solution of the implicitly discretised fluid flow equations by operator-splitting. Journal of Computational Physics 62, 40–65.

[28] Jacobsen, N.G., Fuhrman, D.R., Fredsøe, J., 2012. A wave generation toolbox for the open-source CFD library: OpenFOAM . International Journal for Numerical Methods in Fluids 70, 1073–1088.

[29] Jin, S., Greaves, D., 2021. Wave energy in the UK: Status review and future perspectives. Renewable and Sustainable Energy Reviews 143, 110932.

[30] Kassiotis, C., Ibrahimbegovic, A., Matthies, H., 2010. Partitioned solutions to fluid-structure interaction problem in application to free-surface flows. European Journal of Mechanics B/Fluids 29, 510–521.

[31] Koshizuka, S., Nobe, A., Oka, Y., 1998. Numerical analysis of breaking waves using the moving particle semi-implicit method. International Journal for Numerical Methods in Fluids 26, 751–769.

[32] Kurniawan, A., Brown, S., Forehand, D., Wolgamot, H., 2021. Wave-structure interactions of flexible bags with elastic tendons: Application to wave energy conversion. Journal of Waterway, Port, Coastal, and Ocean Engineering 147, 04020045.

[33] Li, F., Huang, L., 2022. A review of computational simulation methods for a ship advancing in broken ice. Journal of Marine Science and Engineering 10.

[34] Liao, K., Hu, C., 2013. A couplied FDM-FEM method for free surface flow interaction with thin elastic plate. J. Mar. Sci. Technol. 18, 1–11.

[35] Liao, K., Hu, C., Sueyoshi, M., 2015. Free surface flow impacting on an elastic structure: Experimentversus numerical simulation. Appl. Ocean Res. 50, 192–208.

[36] Lind, S., Rogers, B., Stansby, P., 2020. Review of smoothed particle hydrodynamics: towards converged lagrangian flow modelling. Proceedings of the Royal Society A 476.

[37] Love, A., 1888. The small free vibrations and deformation of a thin elastic shell. Philosophical transactions of the royal society of London. (A.) 179, 491–546.

[38] Marón, A., Kapsenberg, G., 2014. Design of a ship model for hydro-elastic experiments in waves. International Journal of Naval Architecture and Ocean Engineering 6, 1130–1147.

[39] Martínez-Ferrer, P., Causon, D., Qian, L., Mingham, C., Ma, Z., 2016. A multi-region coupling scheme for compressible and incompressible flow solvers for two-phase flow in a numerical wave tank. Computers and Fluids 125, 116–129.

[40] Martínez-Ferrer, P., Qian, L., Ma, Z., Causon, D., Mingham, C., 2018. An efficient finite-volume method to study the interaction of two-phase fluid flows with elastic structures. Journal of Fluids and Structures 83, 54–71.

[41] Michler, C., Hulshoff, S., van Bummelen, E., de Borst, R., 2004. A monolithic approach to fluid–structure interaction. Computers & Fluids 33, 839–848.

[42] Montiel, F., Bonnefoy, F., Bennetts, L., Squire, V., Marsault, P., 2013. Hydroelastic response of floating elastic discs to regular waves. part 1. wave basin experiments. Journal of Fluid Mechanics 723, 604–628.

[43] O'Connor, J., Rogers, B., 2021. A fluid-structure interaction model for free-surface flows and flexible structures using smoothed particle hydrodynamics on a GPU. Journal of Fluids and Structures 104.

[44] OpenFOAMWiki, 2019. Extend-bazaar. `https://openfoamwiki.net/index.php/Extend-bazaar`, Last Accessed: 24 Feb 2022.

[45] Panciroli, R., Porfiri, M., 2014. Hydroelastic impact of piezoelectric structures. International Journal of Impact Engineering 66, 18–27.

[46] Piro, D., Maki, K., 2013. Hydroelastic analysis of bodies that enter and exit water. Journal of Fluids and Structures 37, 134–150.

[47] Ransley, E., 2015. Survivability of Wave Energy Converter and Mooring Coupled System using CFD. Ph.D. thesis. University of Plymouth.

[48] Ransley, E., Yan, S., Brown, S., Hann, M., Graham, D., Windt, C., Schmitt, P., Davidson, J., Ringwood, J., Musiedlak, P.H., Wang, J., Wang, J., Ma, Q., Xie, Z., Zhang, N., Zheng, X., Giorgi, G., Chen, H., Lin, Z., Qian, L., Ma, Z., Bai, W., Chen, Q., Zang, J., Ding, H., Cheng, L., Zheng, J., Gu, H., Gong, X., Liu, Z., Zhuang, Y., Wan, D., Bingham, H., Greaves, D., 2020. A blind comparative study of focused wave interactions with floating structures (CCP-WSI Blind Test Series 3). International Journal of Offshore and Polar Engineering 30, 1–10.

[49] Ransley, E., Yan, S., Brown, S., Mai, T., Graham, D., Ma, Q., Musiedlak, P.H., Engsig-Karup, A., Eskilsson, C., Li, Q., Wang, J., Xie, Z., Sriram, V., Stoesser, T., Zhuang, Y., Li, Q., Wan, D., Chen, G., Chen, H., Qian, L., Ma, Z., Mingham, C., Causon, D., Gatin, I., Jasak, H., Vukčević, V., Downie, S., Higuera, P., Buldakov, E., Stagonas, D., Chen, Q., Zang, J., Greaves, D., 2019. A blind comparative study of focused wave interactions with a fixed FPSO-like structure (CCP-WSI Blind Test Series 1). International Journal of Offshore and Polar Engineering 29, 113–127.

[50] Ringsberg, J., Heggelund, S., Lara, P., Jang, B.S., Hirdaris, S., 2017. Structural response analysis of slamming impact on free fall lifeboats. Marine Structures 54, 112–126.

[51] Riyansyah, M., Wang, C., Choo, Y., 2010. Connection design for two-floating beam system for minimum hydroelastic response. Marine Structures 23, 67–87.

[52] Rusche, H., 2002. Computational fluid dynamics of dispersed two-phase flows at high phase fractions. Ph.D. thesis. Imperial College of Science, Technology & Medicine.

[53] Sendil, U., Graf, W., 1974. Transmission of regular waves past floating plates. Coastal Engineering Proceedings 1, 112.

[54] Sree, D., Wing-Keung Law, A., Shen, H., 2017. An experimental study on the interactions between surface waves and floating viscoelastic covers. Wave Motion 70, 195–208.

[55] Stokes, G.G., 1847. On the theory of oscillatory waves. Transactions of the Cambridge Philosophical Society 8, 441–455.

[56] Tuković, Z., Cardiff, P., Karač, A., Jasak, H., Ivanković, 2014. OpenFOAM library for fluid structure interaction, in: 9th OpenFOAM Workshop, Zagreb, Croatia.

[57] Tuković, Z., Jasak, H., 2007. Updated Lagrangian finite volume solver for large deformation dynamic response of elastic body. Transactions of FAMENA 31, 55–70.

[58] Tully, S., Viola, I., 2016. Reducing the wave induced loading of tidal turbine blades through the use of a flexible blade., in: 16th International Symposium on Transport Phenomena and Dynamics of Rotating Machinery, Honolulu, USAl.

[59] Wang, L., Liu, X., Kolios, A., 2016. State of the art in the aeroelasticity of wind turbine blades: Aeroelastic modelling. Renewable and Sustainable Energy Reviews 64, 195–210.
[60] Wang, Y., Wu, W., Guedes Soares, C., 2020. Experimental and numerical study of the hydroelastic response of a river-sea-going container ship. Journal of Marine Science and Engineering 8.
[61] Widlund, O., 1988. Iterative substructuring methods: algorithms and theory for elliptic problems in the plane, in: First International Symposium on Domain Decomposition Methods for Partial Differential Equations, SIAM, Paris, France. pp. 113–128.
[62] Windt, C., Davidson, J., Ringwood, J., 2018. High-fidelity numerical modelling of computational fluid dynamics-based numerical wave tanks. Renewable and Sustainable Energy Reviews 93, 610–630.
[63] Wu, C., Watanabe, E., Utsunomiya, T., 1995. An eigenfunction expansion-matching method for analyzing the wave-induced responses of an elastic floating plate. Applied Ocean Research 17, 301–310.
[64] Xie, F., Zhao, W., Wan, D., 2021. MPS-DEM coupling method for interaction between fluid and thin elastic structures. Ocean Engineering 236.
[65] Yeh, N., Yeh, P., Chang, Y.H., 2015. Artificial floating islands for environmental improvement. Renewable and Sustainable Energy Reviews 47, 616–622.
[66] Zhang, G., Zhao, W., Wan, D., 2022. Moving Particle Semi-implicit method coupled with Finite Element Method for hydroelastic responses of floating structures in waves. European Journal of Mechanics -B/Fluids 95, 63–82.